Model-assisted validation of a strain-based dense sensor network

Jin Yan, Xiaosong Du, Simon Laflamme, Leifur Leifsson, Chao Hu, et al.

Jin Yan, Xiaosong Du, Simon Laflamme, Leifur Leifsson, Chao Hu, An Chen, "Model-assisted validation of a strain-based dense sensor network," Proc. SPIE 10970, Sensors and Smart Structures Technologies for Civil, Mechanical, and Aerospace Systems 2019, 109702C (27 March 2019); doi: 10.1117/12.2515232

SPIE.

Event: SPIE Smart Structures + Nondestructive Evaluation, 2019, Denver, Colorado, United States

Model-assisted validation of a strain-based dense sensor network

Jin Yan[a], Xiaosong Du[b], Simon Laflamme[a,c], Leifur Leifsson[b], Chao Hu[c,d], and An Chen[a]

[a]Department of Civil, Construction and Environmental Engineering, Iowa State University, Ames, IA, 50010, USA
[b]Department of Aerospace Engineering, Iowa State University, Ames, IA, 50010, USA
[c]Department of Electrical and Computer Engineering, Iowa State University, Ames, IA, 50010, USA
[d]Department of Mechanical Engineering, Iowa State University, Ames, IA, 50010, USA

ABSTRACT

Recent advances in sensing are empowering the deployment of inexpensive dense sensor networks (DSNs) to conduct structural health monitoring (SHM) on large-scale structural and mechanical systems. There is a need to develop methodologies to facilitate the validation of these DSNs. Such methodologies could yield better designs of DSNs, enabling faster and more accurate monitoring of states for enhancing SHM. This paper investigates a model-assisted approach to validate a DSN of strain gauges under uncertainty. First, an approximate physical representation of the system, termed the physics-driven surrogate, is created based on the sensor network configuration. The representation consists of a state-space model, coupled with an adaptive mechanism based on sliding mode theory, to update the stiffness matrix to best match the measured responses, assuming knowledge of the mass matrix and damping parameters. Second, the physics-driven surrogate model is used to conduct a series of numerical simulations to map damages of interest to relevant features extracted from the synthetic signals that integrate uncertainties propagating through the physical representation. The capacity of the algorithm at detecting and localizing damages is quantified through probability of detection (POD) maps. It follows that such POD maps provide a direct quantification of the DSNs' capability at conducting its SHM task. The proposed approach is demonstrated using numerical simulations on a cantilevered plate elastically restrained at the root equipped with strain gauges, where the damage of interest is a change in the root's bending rigidity.

Keywords: Structural health monitoring, dense sensor network, strain, sliding mode observer, probability of detection

1. INTRODUCTION

Structural health monitoring (SHM) is the automation of the structural integrity assessment task. Of interest to this paper are SHM strategies based on dense sensor networks (DSNs), which have recently been empowered through advances in smart materials and signal processing.[1–4] The promise of DSNs lies in their high spatial resolution that yields rich spatio-temporal information about the monitored component.[5] If properly harnessed through strategically tailored signal processing algorithms, such information could dramatically improve structural condition assessment capabilities, directly enabling condition-based maintenance decisions.

However, linking monitoring data to decisions is not an easy task. The condition assessment capabilities highly depends on the quality of the integrated design of the SHM solution, which is hard to evaluate. In this paper, we propose a framework for the validation of DSN design, therefore enabling the optimization of DSN configurations, including the number of sensing units and their locations within a network. The methodology leverages a physical surrogate model that gets updated from field data. The idea of numerical model updating is not new. There exist several examples in the literature of model updating based on vibration data to relate to changes in stiffness.[6–8] However, such model updating techniques are difficult to apply, because they require computationally

Further author information: (Send correspondence to Jin Yan)
Jin Yan: E-mail: yanjin@iastate.edu, Telephone: 1 470 428 1728

Sensors and Smart Structures Technologies for Civil, Mechanical, and Aerospace Systems 2019, edited by Jerome P. Lynch, Haiying Huang, Hoon Sohn, Kon-Well Wang,Proc. of SPIE Vol. 10970, 109702C
 · doi: 10.1117/12.2515232

appropriate optimization procedures, precise numerical models, uncertainty quantification, etc.[9–11] A solution is to leverage iterative procedures and simplified models that are more applicable in real-time, yet at the cost of lower accuracy.[12,13]

Here, the physical surrogate is a simplified representation of the monitored system that is constructed based on a given DSN configuration. The performance of the DSN is quantified using the probability of detection (POD) metric,[14,15] which allows assessing the capability of a DSN to quantify damage in an uncertain environment. Originally developed for nondestructive evaluation applications, the concept of POD has been extended to SHM applications.[16] For instance, Kabban et al.[17] proposed a statistical method for analyzing dependent measurements and demonstrated the method on a representative aircraft structural component. Forsyth et al.[18] investigated how POD could be generated from multiple sets of repeated measurements.

Work presented in this paper is a continuation of preliminary studies.[19,20] We use the physical surrogate model to compute POD (or Model Assisted POD - MAPOD) based on user-defined detection requirements and algorithms. The application of interest is a strain-based DSN previously developed by the authors. The remainder of the paper is organized as follows. Section 2 describes the DSN assessment framework, including a description of the DSN of interest, the construction of the reference model and its adaptation, and the MAPOD process. Section 3 presents and discusses results from numerical simulations conducted on a cantilevered plate to verify the proposed framework. Section 4 concludes the paper.

2. DENSE SENSOR NETWORK ASSESSMENT FRAMEWORK

The proposed DSN assessment framework is illustrated in Figure 1. For a DSN measuring strain (Sect. 2.1) ε produced by an input acting on the monitored dynamic system, a least squares estimator (LSE) algorithm is used to fit strain data and extract displacement and velocity states $\mathbf{X}$. States $\mathbf{X}$ along with their estimations from the reference model, denoted by the hat, are used to update a reference model (Sect. 2.2), here using sliding mode theory (Sect. 2.3). After the reference model is appropriately updated, it is used to create a responses bank by simulating uncertainties of interest in the reference model. Note that such a bank requires the including of a user-defined damage discovery algorithm that links signal to damage assessment. This response bank is used in generating the POD metrics (Sect. 2.4) to quantify the performance of the DSN configuration.

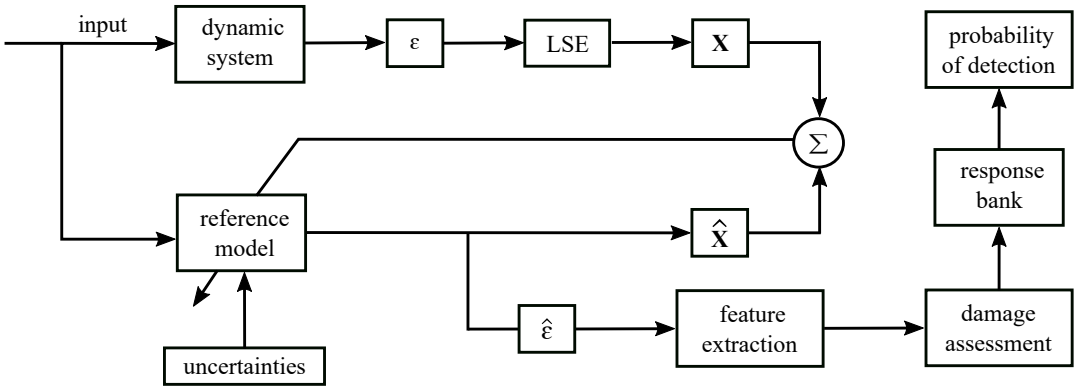

Figure 1. Schematic of the DSN assessment framework.

2.1 Strain-based Dense Sensor Network

In this paper, the DSN of interest consists of a network of flexible electronics, termed soft elastomeric capacitors (SECs), previously proposed by the authors. The SEC technology is a low-cost large area electronics suitable for strain sensing over large-scale surfaces. Figure 2(a) shows a picture of an SEC measuring 3 x 3 in^2. Details on the fabrication process and derivation of the electromechanical model can be found in Reference.[21] Briefly, the capacitance (C) of an SEC can be estimated from the equation for a parallel plate capacitor assuming a low sampling rate (< 1000 Hz):

$$C = \varepsilon_0 \varepsilon_r \frac{A}{h} \tag{1}$$

where ε_0 is the vacuum permittivity ($\varepsilon_0 = 8.854$ pF/m), ε_r is the relative permittivity of the dielectric, A is the electrode's surface area of width d and length l, and h is the thickness of the dielectric, as illustrated in Figure Fig. 2(b). Assuming small strain, Equation 1 can be written:

$$\frac{\triangle C}{C_0} = \lambda(\varepsilon_x + \varepsilon_y) \tag{2}$$

where $\lambda \approx 2$ is the gauge factor, and ε_x and ε_y are the strains along the x and y planes, respectively. It follows from Equation 2 that the sensor measures the additive in-plane strain. Applications of the SEC in DSN configurations are demonstrated in References,[4,22] which demonstrations include the decomposition of measurements into unidirectional strain maps.

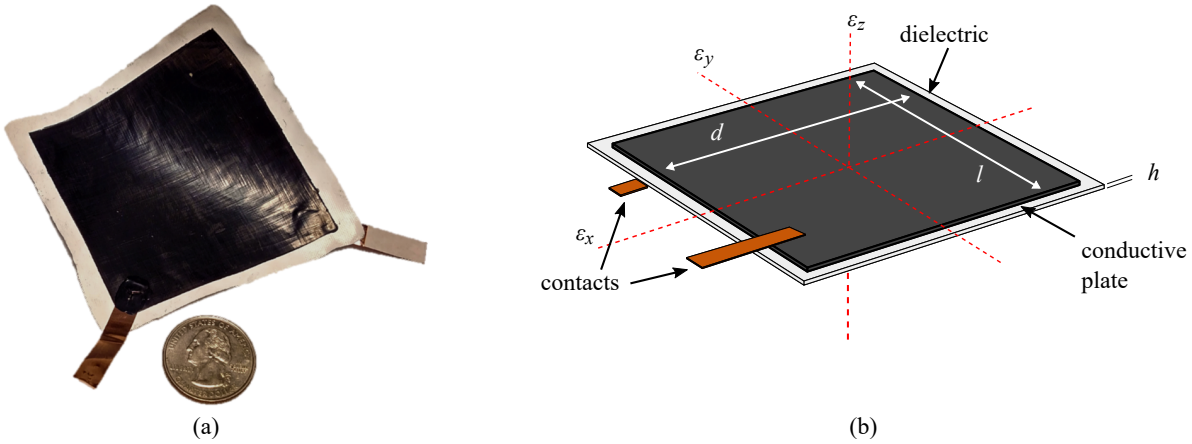

Figure 2. (a) picture of an SEC; and (b) SEC schematic with key components annotated.

2.2 Reference Model

The reference model is constructed as a linear system of the following form

$$\mathbf{M}\ddot{\mathbf{q}}(t) + \mathbf{D}\dot{\mathbf{q}}(t) + \mathbf{K}\mathbf{q}(t) = \mathbf{B}_f\mathbf{f}(t) \tag{3}$$

where t denotes time, the dot a time derivative, $\mathbf{q}(t) \in \mathbb{R}^{n\times 1}$ the displacement vector, $\mathbf{M} \in \mathbb{R}^{n\times n}, \mathbf{D} \in \mathbb{R}^{n\times n}$, and $\mathbf{K} \in \mathbb{R}^{n\times n}$ the mass, proportional damping, and stiffness matrices, respectively, $\mathbf{B}_f \in \mathbb{R}^{n\times n}$ the force application vector, and $\mathbf{f}(t) \in \mathbb{R}^{n\times 1}$ the vector of external forces for an n degrees-of-freedom (nDOF) representation. The dynamic parameter matrices are constructed following a finite element method as a function of sensor locations, presented in Sect. 3.

Equation 3 is adapted in a state space formulation

$$\begin{aligned} \dot{\mathbf{X}} &= \mathbf{A}\mathbf{X} + \mathbf{B}\mathbf{f} \\ \mathbf{Y} &= \mathbf{C}\mathbf{X} \end{aligned} \tag{4}$$

where $\mathbf{X} = [\mathbf{q}, \dot{\mathbf{q}}]^{\mathrm{T}}$ is the state vector, $\mathbf{Y}$ is the measurement output, and $\mathbf{C}$ the observation matrix, with

$$\mathbf{A} = \begin{bmatrix} \mathbf{0} & \mathbf{I} \\ -\mathbf{M}^{-1}\mathbf{K} & -\mathbf{M}^{-1}\mathbf{D} \end{bmatrix}, \mathbf{B} = \begin{bmatrix} \mathbf{0} \\ -\mathbf{M}^{-1} \end{bmatrix} \tag{5}$$

and $\mathbf{C}$ will be defined later for strain measurements.

2.3 Model Adaptation

The reference model is sequentially updated from measurement inputs using sliding mode theory. Assume that the system's stiffnesses $\mathbf{K}$ are the only adjustable parameters, and consider the real system and estimated systems:

$$\begin{aligned} \dot{\mathbf{X}} &= \mathbf{A}\mathbf{X} + \mathbf{B}\mathbf{f} \\ \dot{\hat{\mathbf{X}}} &= \hat{\mathbf{A}}\hat{\mathbf{X}} + \mathbf{B}\mathbf{f} \end{aligned} \tag{6}$$

with

$$\hat{\mathbf{A}} = \begin{bmatrix} \mathbf{0} & \mathbf{I} \\ -\mathbf{M}^{-1}\hat{\mathbf{K}} & -\mathbf{M}^{-1}\mathbf{D} \end{bmatrix} \tag{7}$$

The error between both systems can be written $\tilde{\mathbf{A}} = \mathbf{A} - \hat{\mathbf{A}}$, where the tilde denotes the estimation error. The estimation error matrix $\tilde{\mathbf{A}}$ can be written $\tilde{\mathbf{A}} = \tilde{\theta}\mathbf{Q}$, where θ is the vector of adjustable parameters, and $\mathbf{Q}$ is the matrix containing the non-adjustable parameters. Consider the sliding surface s

$$s = \left(\frac{d}{dt} + c\right)\mathbf{e} = \mathbf{P}\mathbf{e} \tag{8}$$

where $\mathbf{e} = \mathbf{X} - \hat{\mathbf{X}}$ is the state error, $\mathbf{P} = [1, c]$ is a user-defined vector, and c is a strictly positive constant, and take the following Lyapunov function

$$\mathbf{V} = \frac{1}{2}(s^2 + \tilde{\theta}\Gamma_\theta^{-1}\dot{\tilde{\theta}}^{\mathrm{T}}) \tag{9}$$

where Γ_θ is the positive definite diagonal matrix representing learning parameters. Function V is positive definite and contains all time-varying parameters. Taking its time derivative and substituting Equations 6, 8 and 9 yields:

$$\begin{aligned} \dot{\mathbf{V}} &= s^{\mathrm{T}}\mathbf{P}\dot{e} + \tilde{\theta}\Gamma_\theta^{-1}\dot{\tilde{\theta}}^{\mathrm{T}} \\ &= s^{\mathrm{T}}\mathbf{P}\left[\mathbf{A}\mathbf{X} - \hat{\mathbf{A}}\hat{\mathbf{X}}\right] + \tilde{\theta}\Gamma_\theta^{-1}\dot{\tilde{\theta}}^{\mathrm{T}} \\ &= s^{\mathrm{T}}\mathbf{P}\left[\mathbf{A}\mathbf{X} - (\mathbf{A} - \tilde{\mathbf{A}})\hat{\mathbf{X}}\right] + \tilde{\theta}\Gamma_\theta^{-1}\dot{\tilde{\theta}}^{\mathrm{T}} \\ &= s^{\mathrm{T}}\mathbf{P}\left[\mathbf{A}\mathbf{e} + \tilde{\mathbf{A}}\hat{\mathbf{X}}\right] + \tilde{\theta}\Gamma_\theta^{-1}\dot{\tilde{\theta}}^{\mathrm{T}} \\ &= \mathbf{e}^{\mathrm{T}}\mathbf{P}^{\mathrm{T}}\mathbf{P}\mathbf{A}\mathbf{e} + s^{\mathrm{T}}\mathbf{P}\tilde{\mathbf{A}}\hat{\mathbf{X}} + \tilde{\theta}\Gamma_\theta^{-1}\dot{\tilde{\theta}}^{\mathrm{T}} \end{aligned} \tag{10}$$

The first term in Equation 10 is negative semi-definite. The adaptation rule is selected such that

$$s^{\mathrm{T}}\mathbf{P}\tilde{\mathbf{A}}\hat{\mathbf{X}} + \tilde{\theta}\Gamma_\theta^{-1}\dot{\tilde{\theta}}^{\mathrm{T}} < 0 \tag{11}$$

Using

$$\dot{\hat{\theta}} = \Gamma_\theta s^{\mathrm{T}}\mathbf{P}\mathbf{Q}\hat{\mathbf{X}} \tag{12}$$

into Equation 10 and noting that $\dot{\tilde{\theta}} = \dot{\theta} - \dot{\hat{\theta}} = -\dot{\hat{\theta}}$ yields

$$\begin{aligned} \dot{\mathbf{V}} &= \mathbf{e}^{\mathrm{T}}\mathbf{P}^{\mathrm{T}}\mathbf{P}\mathbf{A}\mathbf{e} + s^{\mathrm{T}}\mathbf{P}\tilde{\mathbf{A}}\hat{\mathbf{X}} - \tilde{\theta}\Gamma_\theta^{-1}(\Gamma_\theta s^{\mathrm{T}}\mathbf{P}\mathbf{Q}\hat{\mathbf{X}}) \\ &= \mathbf{e}^{\mathrm{T}}\mathbf{P}^{\mathrm{T}}\mathbf{P}\mathbf{A}\mathbf{e} + s^{\mathrm{T}}\mathbf{P}\tilde{\mathbf{A}}\hat{\mathbf{X}} - s^{\mathrm{T}}\mathbf{P}\tilde{\mathbf{A}}\hat{\mathbf{X}} \\ &= \mathbf{e}^{\mathrm{T}}\mathbf{P}^{\mathrm{T}}\mathbf{P}\mathbf{A}\mathbf{e} \end{aligned} \tag{13}$$

showing the stability of the adaptation rule (Equation 12) under persistent excitation.[23,24] In the discrete time form, Equation 12 becomes:

$$\theta_{k+1} = \theta_k - \Gamma_\theta \Delta t s^{\mathrm{T}} \mathbf{P}\mathbf{Q}\hat{\mathbf{X}}_k \tag{14}$$

2.4 Model Assisted Probability of Detection

MAPOD is used to quantify the performance of a given DSN. The process starts by defining the uncertain model parameters as random variables with specific probability distributions. Here, we consider the aleatory uncertainties from the applied load and sensor noise. Uncertainties are introduced in the updated reference model, and several realizations are generated. For each damage case, maps of dimension $\mathbb{R}^{a\times m}$ are produced, where a is the number of sensors and m is the number of sample points, and concatenated in a response bank.

After, sensor measurements are linked to a damage indicator through a user-defined damage discovery algorithm. Here, for illustrative purposes, we use a simple algorithm that discovers damage based on signal differences over a period T, assuming a stationary load. To do so, strain measurements are segmented into different streams $\mathbf{S}$ with a size of $\mathbb{R}^{a\times m}$. Let $\mathbf{S}^k$ denote the kth stream of the signal. The damage indicator J is defined by the difference between the initial stage $\mathbf{S}^0$ (assumed as "healthy") and current measurements $\mathbf{S}^k$

$$J = \frac{1}{T}\sum_{i=1}^{a}\sum_{j=1}^{m}\left|\mathbf{S}_{ij}^k - \mathbf{S}_{ij}^0\right| \tag{15}$$

Lastly, the MAPOD process is conducted by constructing the J - α plot where α is the damage severity by drawing the samples and using linear regression to plot the damage indicator versus the degree of damage

$$\ln\hat{\alpha} = \beta_0 + \beta_1 \ln\alpha + \epsilon \tag{16}$$

where coefficients β_0 and β_1 can be determined by a least squares estimator, and the ϵ has a Normal distribution $\mathcal{N}(0, \sigma_\epsilon^2)$ with zero mean and standard deviation σ_ϵ. For a given threshold $\bar{\alpha}$, the POD is computed as follows:

$$\mathrm{POD}(\alpha) = P(\log(\alpha) > \bar{\alpha}) = 1 - \Phi\left(\frac{\log\bar{\alpha} - \beta_0 + \beta_1\log\alpha}{\sigma_\epsilon}\right) \tag{17}$$

3. RESULTS AND DISCUSSION

3.1 Numerical Model

The DSN assessment framework is verified through numerical simulations of a cantilevered plate of length $l_x = 276$ mm, width $l_y = 33$ mm, and thickness $l_h = 1$ mm, illustrated in Figure 3. The plate is Grade 316 stainless steel, with an assigned Young's modulus $E = 193$ GPa, density $\rho = 8027\mathrm{kg/m}^3$, and Poisson's ratio $\nu = 0.3$.

The study starts with the plate virtually equipped with five SECs, and synthetic data were produced in `MATLAB` by discretizing the plate into 100 elements and applying a point load at the tip. This `MATLAB` model is taken as the real or true system. A white noise excitation with a bandwidth of 100 Hz and magnitude of 20 N (Figure 3(b)) was used to produce synthetic measurements $\mathbf{S}^0$ for the reference model verification stage, and a harmonic excitation of magnitude 10 N and frequency of 5 rad/s (Figure 3(c)) was used for the MAPOD-based DSN assessment. An arbitrary 20% Gaussian noise was added to the simulated measurements.

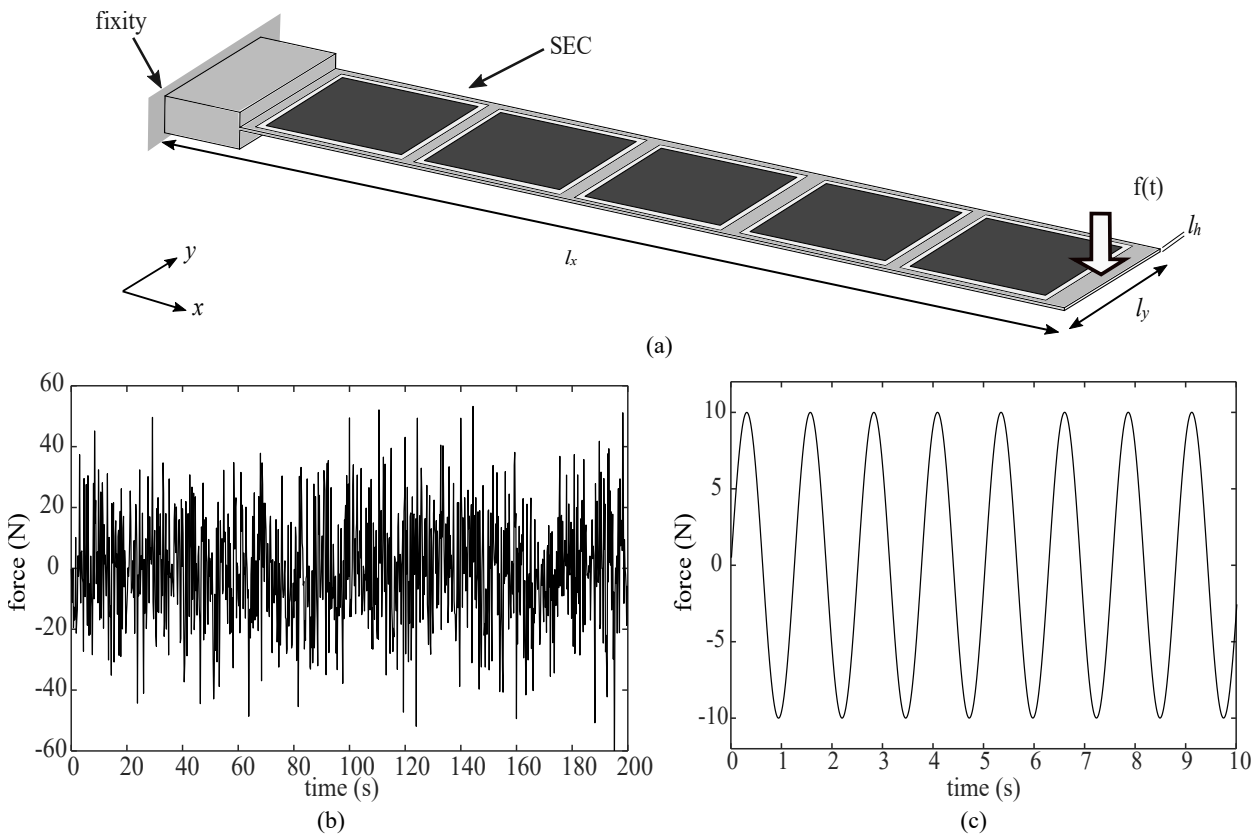

Figure 3. (a) Virtual system under investigation; (b) white noise excitation; and (c) harmonic excitation.

3.2 Reference Model Verification

The reference model was discretized into six elements, consistent with the number of SECs installed plus an additional element linking to the fixity. The system's matrices were constructed by assembling the element mass $\mathbf{M}_e$, stiffness $\mathbf{K}_e$, and damping $\mathbf{D}_e$ matrices

$$\begin{aligned}
\mathbf{M}_e &= \frac{\rho A l}{420}\begin{bmatrix} 156 & 22l & 54 & -13l \\ 22l & 4l^2 & 13l & -3l^2 \\ 54 & 13l & 156 & -22l \\ -13l & -3l^2 & -22l & 4l^2 \end{bmatrix} \\
\mathbf{K}_e &= \frac{EI}{l^3}\begin{bmatrix} 12 & 6l & -12 & 6l \\ 6l & 4l^2 & -6l & 2l^2 \\ -12 & -6l & 12 & -6l \\ 6l & 2l^2 & -6l & 4l^2 \end{bmatrix} \\
\mathbf{D}_e &= \eta \mathbf{K}^e
\end{aligned} \tag{18}$$

where, for each element, A is the cross-sectional area, l is the length, I is the moment of inertia, and $\eta = 0.0001$ is the stiffness proportionality term. Each element comprises two DOFs at each end, one translational and one rotational, as illustrated in Figure 4. This gives rise to the following state vector

$$\mathbf{X}_e = \begin{bmatrix} q_{1,1} & q_{1,2} & q_{2,1} & q_{2,2} & \dot{q}_{1,1} & \dot{q}_{1,2} & \dot{q}_{2,1} & \dot{q}_{2,2} \end{bmatrix}^{\mathrm{T}} \tag{19}$$

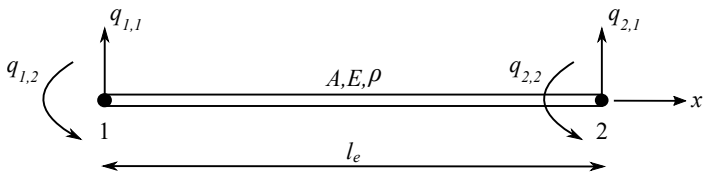

Figure 4. One element displacement notation.

and the element observation matrix $\mathbf{C}_e$ is constructed for strain measurement

$$\mathbf{C}_e = \frac{l_h}{2l}\begin{bmatrix}0 & -1 & 0 & 1\end{bmatrix}^{\mathrm{T}} \tag{20}$$

The assembled state vector $\mathbf{X}$ has a total of 24 states. To verify the reference model updating mechanism, a time history of measurements was produced while changing the bending rigidity of the fixity (element one) by 20% between simulation time $t = 60$ and $t = 120$ sec. The state space matrix $\mathbf{A}$ was updated by searching parameter θ that pre-multiplies bending rigidity EI for that element, with

$$\tilde{\mathbf{A}} = -\theta\begin{bmatrix}\mathbf{M}_1^{-1}\mathbf{K}_1 & \cdots & 0 & \eta\mathbf{M}_1^{-1}\mathbf{K}_1 & \dots & 0\\ \vdots & \ddots & \vdots & \vdots & \ddots & \vdots\\ 0 & \cdots & 0 & 0 & \cdots & 0\end{bmatrix} \tag{21}$$

The displacement and velocity feedback used in the adaptation rule is obtained from the measured strain by fitting and integrating spatial strain measurements using a kth order polynomial function $\varepsilon = \xi_0 + \sum_{j=1}^{k}\xi_j x^j$. For this study, a polynomial of size $k = 3$ was utilized. The fitting coefficients ξ_j are obtained through a least squares estimator

$$\xi = (\mathbf{H}^{\mathrm{T}}\mathbf{H})^{-1}\mathbf{H}^{\mathrm{T}}\varepsilon \tag{22}$$

where $\mathbf{H}$

$$\mathbf{H} = \begin{bmatrix}1 & x_1 & x_1^2 & x_1^3\\ 1 & x_2 & x_2^2 & x_2^3\\ \vdots & \vdots & \vdots & \\ 1 & x_5 & x_5^2 & x_5^3\end{bmatrix} \tag{23}$$

Integrating Equation 23 and assigning the proper boundary conditions yield an expression for $\mathbf{q}$

$$\mathbf{q} = -\frac{2}{l_h}\begin{bmatrix}x_1 & \frac{1}{2}x_1^2 & \frac{1}{3}x_1^3 & \frac{1}{4}x_1^4\\ \frac{1}{2}x_1 & \frac{1}{6}x_1^2 & \frac{1}{12}x_1^3 & \frac{1}{20}x_1^4\\ \frac{1}{2}x_2 & \frac{1}{6}x_2^2 & \frac{1}{12}x_2^3 & \frac{1}{20}x_2^4\\ \vdots & \vdots & \vdots & \vdots\\ x_5 & \frac{1}{2}x_5^2 & \frac{1}{3}x_5^3 & \frac{1}{4}x_5^4\\ \frac{1}{2}x_5 & \frac{1}{6}x_5^2 & \frac{1}{12}x_5^3 & \frac{1}{20}x_5^4\end{bmatrix}\begin{bmatrix}\xi_1\\ \xi_1\\ \xi_2\\ \vdots\\ \xi_5\\ \xi_5\end{bmatrix} \tag{24}$$

In this paper, the learning rate Γ_θ was set to $1e^{-10}$, and c was set to be 2 for the adaptation mechanism. Figure 5 plots the results from the adaptation, showing the estimated (red dashed line) versus real (black solid line) bending rigidity (Figure 5(a)) and the estimation error between referenced model strain $\hat{\varepsilon}$ and measured strain ε (Figure 5(b)). The offset between the estimated and real bending rigidities is attributed to the level

of noise in the sensor, observable in the strain difference time histories, to the LSE algorithm used to convert strain into displacements and velocities, and to the level of simplification using six elements for constructing the simplified physical surrogate model. Nevertheless, the algorithm was capable of tracking changes in bending rigidity, which can be used as a measure of damage.

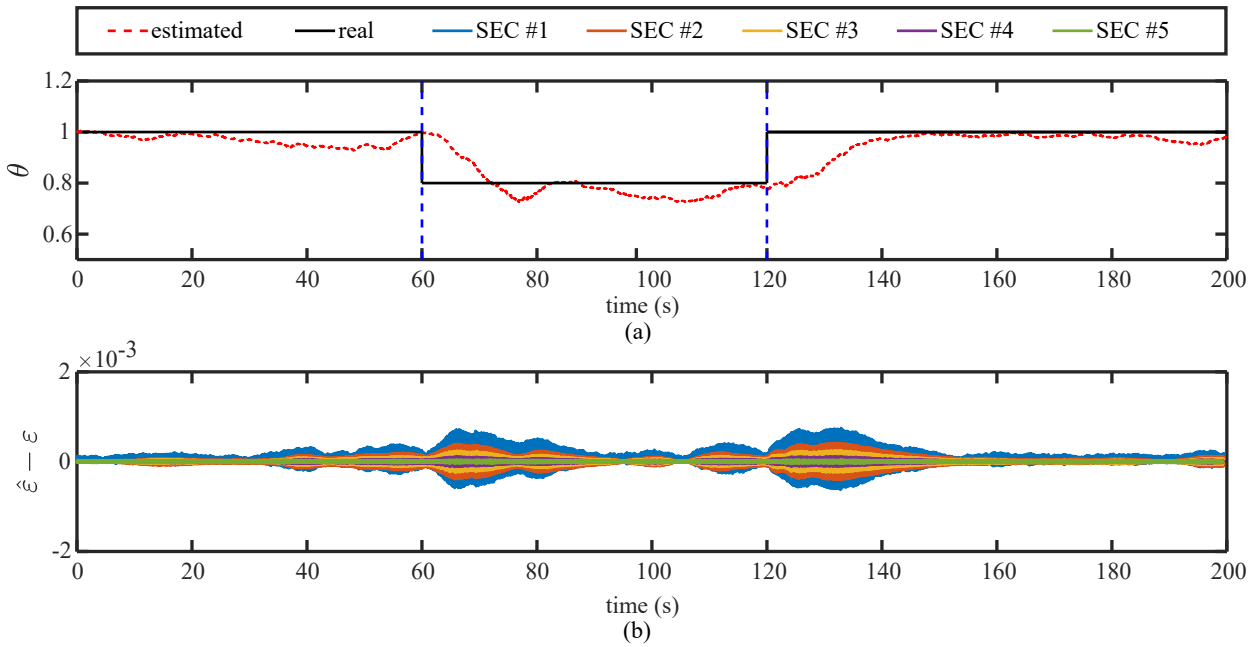

Figure 5. (a) adaptation mechanism performance; (b) adapted output tracking error in presence of parameter variation.

3.3 Model Assisted Probability of Detection

We verify the proposed framework by assessing the performance of the DSN configuration using MAPOD and subjecting the plate to a harmonic load at its tip. Two sources of uncertainties were considered. One is an uncertainty on the input, where a Gaussian variation of 10% was added to its magnitude. The other is an uncertainty an the strain measurements, with the 20% added Gaussian noise. A total of 20 damage patterns were simulated by reducing the bending rigidity of the fixity to represent damage at the cantilever root. Damage cases were generated by reducing the bending rigidity randomly between $\alpha = 0.02$ and $\alpha = 0.4$. Damage is considered "discovered" when the damage indicator J becomes larger than the threshold value $J = 1e^{-5}$. The analysis conducted using 1000 realizations of synthetic data sets for each damage. The Latin hypercube sampling technique[25] was used to produce independent samples from the uncertainty distributions.

Figure 6(a) is the $J - \alpha$ plots showing the simulated values, linear regression, 95 % confidence bounds on the linear regression, and damage detection bound. Figure 6(b) is the resulting POD plot and the black curve represents the upper (conservative) 95% confidence bound of the linear regression. Results show that for the particular DSN configuration and damage detection algorithm, there is a 50% probability with 95% confidence of detecting a change of bending rigidity greater than $\alpha_{50/95} = 0.081$ at the cantilever's root (bottom black dashed arrow), and a 90% probability with 95% confidence of detecting a change greater than $\alpha_{90/95} = 0.113$ (upper black dashed arrow).

The DSN assessment procedure is repeated on different DSN configurations to demonstrate how the proposed framework can be leveraged in designing a DSN. A total of six DSN scenarios were considered: 5, 6, 7, 8, 9 and 10 SECs. Figure 7(a) illustrates the DSN configuration with 5, 7 and 10 SECs. POD curves were generated using the same methodology as for the five SECs. Figure 7(b) reports the resulting POD surface plot for damage detection with a 95% confidence. Results in Figure 7(c) shows that, by increasing the resolution of the network,

the 90% damage detection with 95% improves substantially from a 11.3% change in bending rigidity using 5 SECs to a 3.1% change in rigidity using 10 SECs.

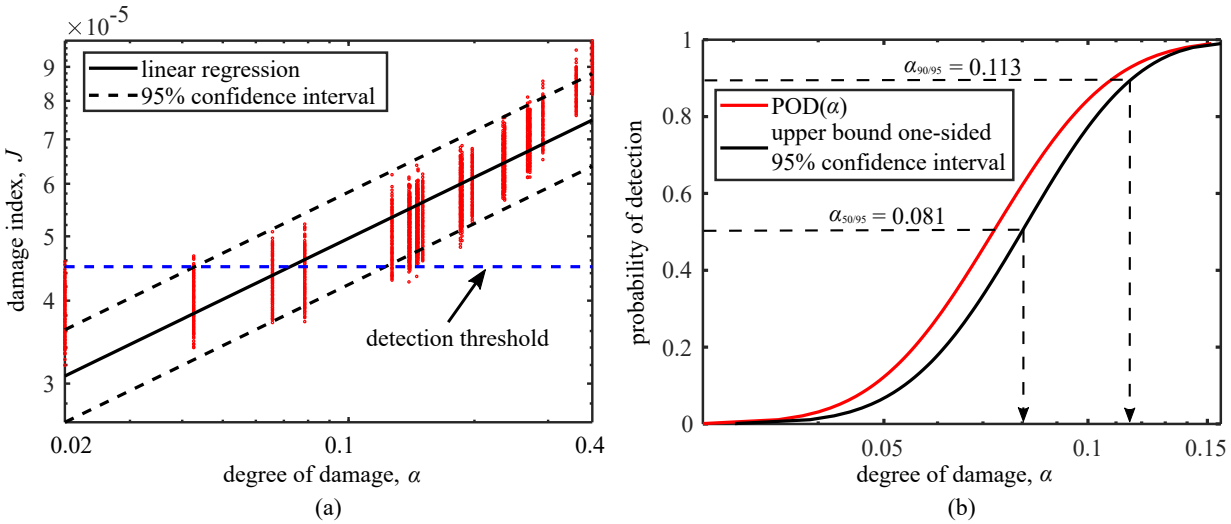

Figure 6. (a) J *vs.* α; and (b) POD plot.

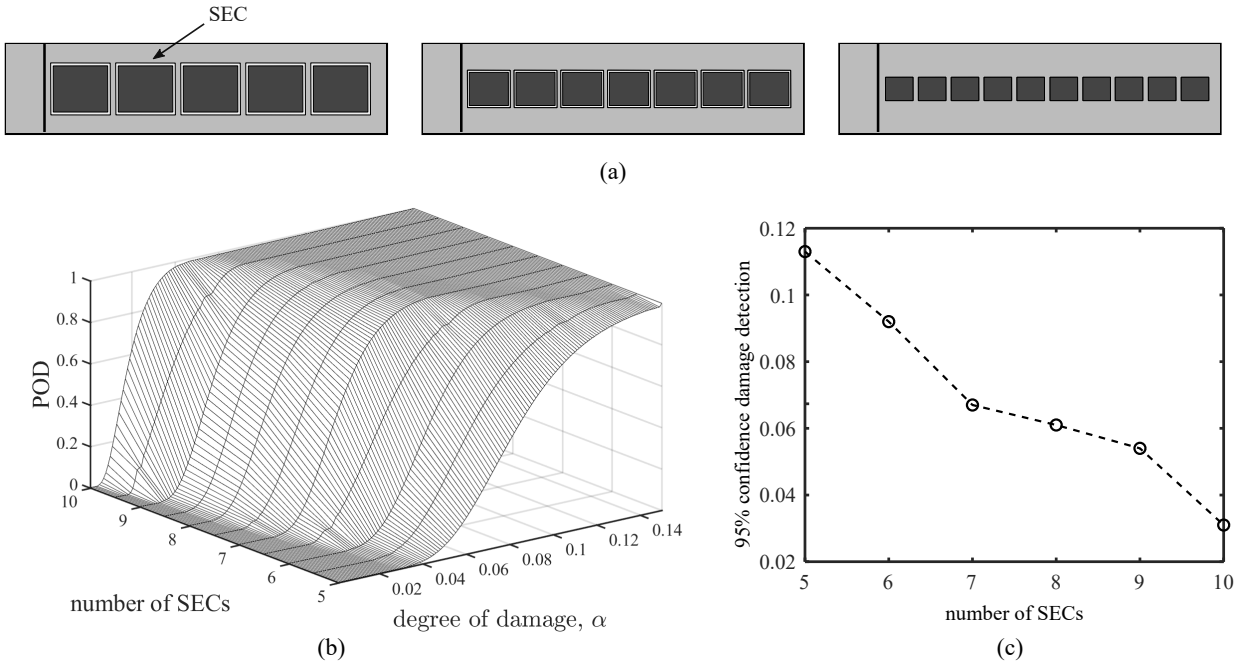

Figure 7. (a) Different DSN configurations under investigation (5 SECs (left), 7 SECs (center), and 10 SECs (right)); and (b) 95% POD surface plots; and (c) 90%/95% damage detection under different DSN configurations.

4. CONCLUSIONS

This paper presented a preliminary investigation of a performance assessment framework for structural health monitoring solutions leveraging dense sensor networks (DSNs). The framework consists of constructing a physical surrogate model based on a given DSN configuration, sequentially adapting the model from field data using sliding

mode theory, and using a model-assisted probability of detection (MAPOD) to assess the DSN's capability at detecting user-defined damage cases of varying degrees of severity.

A numerical study was conducted to verify and demonstrate the framework on a simple cantilevered plate equipped with a DSN measuring strain. Uncertainties considered in the model included uncertainties in the applied load and sensor noise. Results showed that MAPOD was capable of assessing the performance of the DSN at detecting damage at the root. Other DSN configurations were considered in the simulations, and the MAPOD-based assessment showed that it was possible to quantify the performance of each DSN configuration.

Such results could be used to conduct a cost-benefit analysis of the SHM system to select an optimal DSN resolution. Future work includes the extension of the framework to two-dimensional systems of arbitrary configuration for which soft elatomeric capacitors could be fully leveraged, and the incorporation of multi-location damage cases.

ACKNOWLEDGMENTS

This research is partially funded by the Air Force Office of Scientific Research (AFOSR) under award number FA9550-17-1-0131, and the American Society for Nondestructive Testing. Their support is gratefully acknowledged. Any opinions, findings, and conclusions or recommendations expressed in this material are those of the authors and do not necessarily reflect the views of the sponsors.

REFERENCES

[1] Lynch, J. P., Wang, Y., Loh, K. J., Yi, J.-H., and Yun, C.-B., "Performance monitoring of the geumdang bridge using a dense network of high-resolution wireless sensors," *Smart Materials and Structures* **15**, 1561–1575 (oct 2006).

[2] Yao, Y. and Glisic, B., "Detection of steel fatigue cracks with strain sensing sheets based on large area electronics," *Sensors* **15**, 8088–8108 (Apr 2015).

[3] Tung, S.-T. and Glisic, B., "Sensing sheet: The response of full-bridge strain sensors to thermal variations for detecting and characterizing cracks," *Measurement Science And Technology* **27**, 124010 (Oct 2016).

[4] Downey, A., Laflamme, S., and Ubertini, F., "Experimental wind tunnel study of a smart sensing skin for condition evaluation of a wind turbine blade," *Smart Materials And Structures* (Oct 2017).

[5] Ubertini, F., Laflamme, S., Chatzi, E., Glisic, B., and Magalhães, F., "Dense sensor networks for mesoscale SHM: Innovations in sensing technologies and signal processing," *Measurement Science and Technology* **28**, 040103 (feb 2017).

[6] Alessandro Cancelli, Simon Laflamme, A. A. S. S. F. U., "Vibration-based damage localization and quantification in a pretensioned concrete girder using stochastic subspace identification and particle swarm model updating," *Structural Health Monitoring* (2019).

[7] Li, D. and Wang, Y., "Sparse sum-of-squares optimization for model updating through minimization of modal dynamic residuals," *Journal of Nondestructive Evaluation, Diagnostics and Prognostics of Engineering Systems* **2**, 011005 (jan 2019).

[8] Yan, J., Downey, A., Cancelli, A., Chen, A., Ubertini, F., Du, X., Laflamme, S., and Leifsson, L., "Surrogate model for condition assessment of structures using a dense sensor network," in [*Sensors and Smart Structures Technologies for Civil, Mechanical, and Aerospace Systems 2018*], Sohn, H., ed., SPIE (mar 2018).

[9] Keyes, D. E., "Exaflop/s: The why and the how," *Comptes Rendus Mécanique* **339**, 70–77 (feb 2011).

[10] Peherstorfer, B., Willcox, K., and Gunzburger, M., "Survey of multifidelity methods in uncertainty propagation, inference, and optimization,"

[11] Benner, P., Ohlberger, M., Cohen, A., and Wilcox, K. E., [*Model Reduction and Approximation: Theory and Algorithms*], SIAM-Society for Industrial & Applied Mathematics (2017).

[12] Benner, P., Gugercin, S., and Willcox, K., "A survey of projection-based model reduction methods for parametric dynamical systems," *SIAM Review* **57**, 483–531 (jan 2015).

[13] Hong, J., Laflamme, S., Cao, L., Dodson, J., and Joyce, B., "Variable input observer for nonstationary high-rate dynamic systems," *Neural Computing and Applications* (dec 2018).

[14] Military and Government Specs & Standards (Naval Publications and Form Center) (NPFC), *Nondestructive Evaluation System Reliability Assessment* (Apr. 2009).

[15] Downey, A., Sadoughi, M., Laflamme, S., and Hu, C., "Incipient damage detection for large area structures monitored with a network of soft elastomeric capacitors using relative entropy," *IEEE Sensors Journal* **18**, 8827–8834 (nov 2018).

[16] Aldrin, J. C., Medina, E. A., Lindgren, E. A., Buynak, C. F., Knopp, J. S., Thompson, D. O., and Chimenti, D. E., "Case studies for model-assisted probabilistic reliability assessment for structural health monitoring," AIP (2011).

[17] Kabban, C. M. S., Greenwell, B. M., DeSimio, M. P., and Derriso, M. M., "The probability of detection for structural health monitoring systems: Repeated measures data," *Structural Health Monitoring: An International Journal* **14**, 252–264 (jan 2015).

[18] Forsyth, D. S., "Structural health monitoring and probability of detection estimation," AIP Publishing LLC (2016).

[19] Yan, J., Downey, A., Cancelli, A., Chen, A., Ubertini, F., Du, X., Laflamme, S., and Leifsson, L., "Surrogate model for condition assessment of structures using a dense sensor network," in [*Sensors and Smart Structures Technologies for Civil, Mechanical, and Aerospace Systems 2018*], Sohn, H., ed., SPIE (mar 2018).

[20] Du, X., Yan, J., Laflamme, S., Leifsson, L., Tesfahunegn, Y., and Koziel, S., "Model-assisted probability of detection for structural health monitoring of flat plates," in [*Lecture Notes in Computer Science*], 618–628, Springer International Publishing (2018).

[21] Laflamme, S., Ubertini, F., Saleem, H., D'Alessandro, A., Downey, A., Ceylan, H., and Materazzi, A. L., "Dynamic characterization of a soft elastomeric capacitor for structural health monitoring," *Journal Of Structural Engineering* **141**, 04014186 (Aug 2015).

[22] Downey, A., Sadoughi, M., Laflamme, S., and Hu, C., "Fusion of sensor geometry into additive strain fields measured with sensing skin," *Smart Materials and Structures* **27**, 075033 (jun 2018).

[23] Astrom, K. J. and Wittenmark, B., [*Adaptive Control (2nd Edition)*], Prentice Hall (1994).

[24] Joyce, B. S., Hong, J., Dodson, J. C., Wolfson, J. C., and Laflamme, S., "Adaptive observers for structural health monitoring of high-rate, time-varying dynamic systems," in [*Structural Health Monitoring, Photogrammetry & DIC, Volume 6*], 109–119, Springer International Publishing (may 2018).

[25] Haddad, R. E., Fakhereddine, R., Lécot, C., and Venkiteswaran, G., "Extended latin hypercube sampling for integration and simulation," in [*Monte Carlo and Quasi-Monte Carlo Methods 2012*], 317–330, Springer Berlin Heidelberg (2013).